The chemical reactivity of the compounds is much greater than the corresponding chlorine analogues. Both *N*-bromo derivatives react with AgCl, forming the respective silver salts and BrCl, and with chloroform, liberating BrCl. As expected, their reactivity does not approach that of $BrOSO_2F$ with covalent chlorides: $BrOSO_2F$ reacts rapidly with $CFCl_3$ at 22 °C, whereas solutions of the new *N*-bromo compounds appear to be stable at 22 °C.

Characterization of the new compounds is given in the experimental section, with the IR, NMR, Raman, and mass spectra being similar to those of the respective analogues $(CF_3SO_2)_2NCl$[11,12] and $(FSO_2)_2NCl$.[13,17,18] Assignment of frequencies to ν_{N-X} in this series is not obvious.

In conclusion, a new method has been found for the preparation of electropositive *N*-bromo derivatives of sulfonimides by reaction of the Hg(II) derivatives with bromine(I) fluorosulfate. The new compounds $(CF_3SO_2)_2NBr$ and $(FSO_2)_2NBr$ should be useful reagents for bromination reactions and for the introduction of the fluoronated sulfonimides into a variety of substrates.

Experimental Section

General Procedures. Reactions and characterizations of compounds were carried out as previously described.[11,19] $BrOSO_2F$,[5] $HN(SO_2F)_2$,[20] and $(CF_3SO_2)_2NH$[11,12] were prepared by literature methods. $Hg[N(SO_2CF_3)_2]$[12] was prepared in an identical manner with that given below for $Hg[N(SO_2F)_2]$, with $(CF_3SO_2)_2NH$ used in place of $HN(SO_2F)_2$.

Preparation of *N*-Bromo Sulfonimides. In a typical preparation, 4.0 g (5.26 mmol) of $Hg[N(SO_2CF_3)_2]_2$ was loaded in a drybox into a 100-mL Pyrex reactor fitted with a glass–Teflon valve. The reactor was then evacuated for 2 h to remove any traces of moisture. The reactor was then cooled to −196 °C, and 1.63 g (9.1 mmol) of $BrOSO_2F$ was added by vacuum transfer. The reactor was allowed to warm to 22 °C and kept at room temperature for 12 h in the dark. The contents of the reactor were agitated by shaking twice during the reaction period. The volatiles were then pumped through a series of cold traps. The −25 °C trap held the desired product $(CF_3SO_2)_2NBr$ (3.02 g, 8.38 mmol) in 92% yield based upon the starting amount of $BrOSO_2F$. A very small amount of Br_2 and a trace of CF_3Br were also recovered.

The preparation of $(FSO_2)_2NBr$ was carried out similarly by using a slight excess of $Hg[N(SO_2F)_2]_2$ over $BrOSO_2F$. Two successive preparations on different scales gave $(FSO_2)_2NBr$ in 91–92% yield.

$(CF_3SO_2)_2NBr$: mp −25 to −24 °C; IR (vapor in equilibrium with liquid, 25 °C) 1459 (s), 1332 (vw), 1242 (vs), 1135 (s), 844 (s), 768 (vw), 640 (w), 599 (ms), 502 (m) cm^{-1}; Raman (solid, −196 °C) 1452 (w), 1248 (vs), 1123 (m), 866 (w), 774 (vs), 643 (m), 574 (vw), 531 (vw), 399 (m), 336 (s), 296 (s), 259 (vs), 171 (ms) cm^{-1}; NMR ($CDCl_3$/$CFCl_3$) −71.9 ppm (s, CF_3); MS, *m/e* (CI/CH_4) 362/360 (MH^+) 100%.

$(FSO_2)_2NBr$: mp −19 to −18 °C; IR (vapor in equilibrium with liquid, 25 °C) 1494 (s), 1236 (s), 897 (s), 830 (s), 646 (m), 561 (s) cm^{-1}; Raman (solid, −196 °C) 1472 (vw), 1445 (vw), 1223 (vs), 926 (w), 835 (m), 650 (ms), 521 (m), 495 (m), 422 (w), 329 (m), 312 (vs), 276 (s), 183 (ms), 173 (m) cm^{-1}; NMR ($CDCl_3$/$CFCl_3$) 53.4 ppm (s, S–F); MS, *m/e* (CI/CH_4) 182 [$(FSO_2)_2NH_2^+$] with Br_2^+ and Br_3^+ as major ions.

Preparation of $Hg[N(SO_2F)_2]_2$. A slight excess of $(SO_2F)_2NH$ (2.40 g, 13.26 mmol) in 10 mL of CF_3CO_2H was added to $Hg(CF_3CO_2)_2$ (2.61 g, 6.12 mmol). The immediate precipitation of $Hg[N(SO_2F)_2]_2$ took place. The reaction mixture was stirred for 20 min at room temperature, and excess CF_3CO_2H was removed under vacuum. The compound was then dried by heating at ~80 °C under vacuum to a constant weight, yielding $Hg[N(SO_2F)_2]_2$ (3.42 g, 6.10 mmol). It is a white hygroscopic solid soluble in CH_3CN and in acetone with reaction to give a brown solution.

$Hg[N(SO_2F)_2]_2$: mp 272 °C dec; IR (solid) 1457 (vs), 1445 (s, sh), 1223 (s), 1196 (s), 1010 (s), 904 (s), 826 (s), 658 (ms), 566 (s), 480 (m) cm^{-1}; NMR (CD_3CN/$CFCl_3$) 52.5 ppm (s, S–F).

Acknowledgment. Support of this research by the Gas Research Institute and the National Science Foundation is gratefully acknowledged.

Registry No. $(CF_3SO_2)_2NBr$, 104715-39-1; $(FSO_2)_2NBr$, 104715-40-4; $Hg[N(SO_2CF_3)_2]_2$, 104715-41-5; $Hg[N(SO_2F)_2]_2$, 104693-53-0; $BrOSO_2F$, 13997-93-8; $(SO_2F)NH$, 14984-73-7; $Hg(CF_3CO_2)_2$, 13257-51-7.

(17) Ruff, J. K. *Inorg. Chem.* **1965**, *4*, 1446.
(18) DesMarteau, D. D.; LeBlond, R. D.; Hossain, S. F.; Nothe, D. *J. Am. Chem. Soc.* **1981**, *103*, 7734.
(19) Thrasher, J. S.; Bauknight, C. W.; DesMarteau, D. D. *Inorg. Chem.* **1985**, *24*, 1598.
(20) Ruff, J. K. *Inorg. Synth.* **1968**, *11*, 138.

Contribution from the Departments of Chemistry, University of Tennessee, Knoxville, Tennessee 37996-1600, and North Carolina State University, Raleigh, North Carolina 27695-8204

Synthesis, Characterization, and Reactivity of Phosphine- and Arsine-Bridged Dirhodium Complexes Containing Bridging Pyrazolate and Triazolate Ligands

Christopher J. Janke,† Louis J. Tortorelli,† James L. E. Burn,† Craig A. Tucker,‡ and Clifton Woods*†

Received July 1, 1986

In recent years there has been considerable interest in the synthesis, characterization, and reactivities of dinuclear complexes containing bidentate bridging ligands with group 15[1] donor atoms.[2] Much of this interest is focused on the class of dinuclear species known as A-frame complexes because of the potential of many of these A-frame complexes to act as homogeneous catalysts and add small molecules in the vacant site opposite the bridgehead group.[3] We have been interested in several aspects of new dirhodium A-frame complexes that contain two bridging bis(diphenylphosphino)methane (dppm), bis(diphenylarsino)methane (dam), or (diphenylarsino)(diphenylphosphino)methane (dapm) ligands.

Dinuclear rhodium complexes that contain bridging pyrazolate ligands have been previously reported,[4] but none of these were of the A-frame type that contained two bridging dppm, dam, or dapm ligands and a pyrazolate derivative at the bridgehead until recently when some $(dpm)_2$-bridged dirhodium complexes of this type were reported.[5] This report appeared in the midst of our investigation of this class of compounds, and due to some overlap of these two investigations, we extended our studies to include several additional complexes. We report herein the results of our investigations involving the synthesis and characterization of some additional dppm, dam, and dapm dirhodium A-frame complexes that contain the triazolate (trz), the pyrazolate (pz), the 4-methylpyrazolate (4mpz), and the 3,5-dimethylpyrazolate (35mpz) anions at the bridgehead position. These complexes have the basic structures I–IV and are listed in Table I.

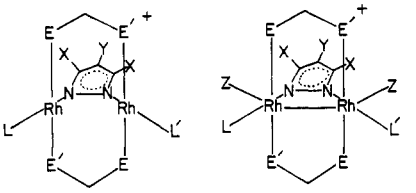

I

III

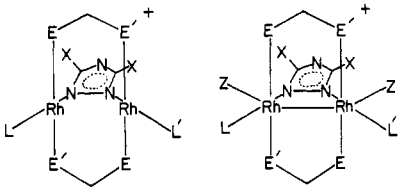

II IV

Experimental Section

Materials. Pyrazole (Hpz), triazole (Htrz), 4-methylpyrazole (H4mpz), 3,5-dimethylpyrazole (H35mpz), *n*-BuLi, and *tert*-butyl isocyanide (*t*-BuNC) were obtained from Aldrich Chemicals. $RhCl_3$ was obtained from Johnson Matthey, Inc., and dppm and dam were purchased from Strem Chemicals. Dapm[6] and $[Rh_2(\mu\text{-dppm})_2(CO)_2(\mu\text{-Cl})]PF_6$[7] were prepared according to literature procedures. Tetrahydrofuran (THF) was freshly distilled from sodium and benzophenone.

† University of Tennessee.
‡ North Carolina State University.

0020-1669/86/1325-4597$01.50/0

Table I. Dinuclear Rhodium(I) Compounds Containing Triazolate and Pyrazolate Derivatives as Bridging Ligands

compd no.	structure	E	E′	L	L′	X	Y	Z
1	I	P	P	CO	CO	H	H	
2	I	P	P	CO	CO	H	CH_3	
3	I	P	P	CO	CO	CH_3	H	
4	II	P	P	CO	CO	H		
5	I	P	P	CO	$CNC(CH_3)_3$	H	H	
6	I	P	P	CO	$CNC(CH_3)_3$	H	CH_3	
7	I	P	P	CO	$CNC(CH_3)_3$	CH_3	H	
8	II	P	P	CO	$CNC(CH_3)_3$	H		
9	I	P	P	$CNC(CH_3)_3$	$CNC(CH_3)_3$	H	H	
10	I	P	P	$CNC(CH_3)_3$	$CNC(CH_3)_3$	H	CH_3	
11	I	P	P	$CNC(CH_3)_3$	$CNC(CH_3)_3$	CH_3	H	
12	II	P	P	$CNC(CH_3)_3$	$CNC(CH_3)_3$	H		
13	I	P	As	CO	CO	H	H	
14	I	P	As	CO	CO	H	CH_3	
15	I	P	As	CO	CO	CH_3	H	
16	IV	P	As	CO	CO	H		
17	I	As	As	CO	CO	H	H	
18	I	As	As	CO	CO	H	CH_3	
19	I	As	As	CO	CO	CH_3	H	
20	IV	As	As	CO	CO	H		
21	III	P	P	CO	CO	H	H	I
22	III	P	P	CO	CO	H	CH_3	I
23	III	P	P	CO	CO	CH_3	H	I
24	IV	P	P	CO	CO	H		I
25	III	P	P	CO	CO	H	Br	Br
26	III	P	P	CO	CO	H	CH_3	Br
27	III	P	P	CO	CO	CH_3	Br	Br
28	III	P	P	CO	CO	H	Cl	Cl
29	III	P	P	CO	CO	H	CH_3	Cl
30	III	P	P	CO	CO	CH_3	Cl	Cl
31	I	P	P	CO	CO	CH_3	Br	
32	I	P	P	CO	CO	CH_3	Cl	

All other solvents were reagent grade and used without further purification.

Preparation of $[Rh_2(\mu\text{-}EE')_2(CO)_2(\mu\text{-}X)]PF_6$ (EE′ = dppm, dam, dapm; X = pz, trz, 4mpz, 35mpz). In a typical reaction, H35dmpz (24.8 mg, 0.258 mmol) in freshly distilled THF was treated with a 2.5 M hexane solution of *n*-BuLi (0.10 mL, 0.250 mmol). Dropwise addition of the 35dmpz solution to $[Rh_2(\mu\text{-dppm})_2(CO)_2(\mu\text{-Cl})]PF_6$ (297 mg, 0.245 mmol) in THF resulted in a color change from yellow to dark orange to reddish orange and finally to red. While the solution was stirred, a precipitate formed. The volume was reduced, and diethyl ether was added. The orange product was filtered and washed with ether and dried in vacuo. The product is readily recrystallized from dichloromethane. The other complexes were prepared in a similar manner; however, some products did not precipitate from the THF solution until ether was added.

Preparation of $[Rh_2(\mu\text{-}EE')_2(CNC(CH_3)_3)_2(\mu\text{-}X)]PF_6$ (EE′ = dppm, dam, dapm; X = pz, 4mpz, 35mpz, trz). In a typical synthesis, $[Rh_2(\mu\text{-dppm})_2(CO)_2(\mu\text{-pz})]PF_6$ (380 mg, 0.306 mmol) was dissolved in 200 mL of degassed acetone under an inert atmosphere. While the acetone solution was stirred, *t*-BuNC (51 mg, 0.611 mmol) was added dropwise. After the mixture was stirred for approximately 1 h, the product was slowly precipitated with a 1:1 mixture of ether and hexanes (mixture of isomers). All other diisocyanide complexes were prepared in a similar manner.

Preparation of $[Rh_2(\mu\text{-}EE')_2(CO)(CNC(CH_3)_3)(\mu\text{-}X)]PF_6$ (EE′ = dppm; X = pz, 4mpz, 35mpz, trz). In a typical preparation, $[Rh_2(\mu\text{-dppm})_2(CO)_2(\mu\text{-35dmpz})]PF_6$ (831 mg, 0.654 mmol) was dissolved in 250 mL of degassed acetone under an inert atmosphere. To the stirred solution was added dropwise *t*-BuNC (54.4 mg, 0.654 mmol). After the mixture was stirred for 1 h, the product was precipitated slowly with degassed ether. The other mixed-carbonyl–isocyanide complexes were prepared in the same manner.

Preparation of $[Rh_2(\mu\text{-dppm})_2I_2(CO)_2(\mu\text{-X})]PF_6$ (X = pz, 4mpz, 35mpz, trz). The following procedure was used to synthesize all iodide complexes. Iodine (0.0136 g, 0.0623 mmol) was added to a stirred solution of $[Rh_2(\mu\text{-dppm})_2(CO)_2(\mu\text{-35dmpz})]PF_6$ (0.0680 g, 0.0535 mmol) in 50 mL of CH_2Cl_2. The resulting red-brown solution was stirred for several minutes and reduced in volume to about 2–4 mL. The red-brown product that precipitated upon the addition of ether was filtered, washed with ether, and dried in vacuo.

Preparation of $[Rh_2(\mu\text{-dppm})_2Br_2(CO)_2(\mu\text{-X})]PF_6$ (X = 4-Bromopyrazolate (4Bpz), 4-Bromo-3,5-dimethylpyrazolate (4B35dmpz), 4mpz). The following synthesis is typical of those used to form the bromo derivatives. To a 100-mL CH_2Cl_2 solution of 155 mg (0.122 mmol) of $[Rh_2(\mu\text{-dppm})_2(CO)_2(\mu\text{-pz})]PF_6$ cooled in ice was slowly added 19.5 mg (0.122 mmol) of Br_2 in 40 mL of CCl_4, with stirring, via a transfer needle. After the addition of Br_2, the solution was stirred for an additional 1 h. The product that precipitated was filtered, and the filtrate was reduced in volume until a second crop of the product began to precipitate. The second crop was filtered, and the filtrate afforded a third crop of product upon the addition of a 1:1 mixture of ether/ligroin. The various crops of product were checked by $^{31}P\{^1H\}$ NMR, and the second crop gave the desired material free of impurities. In the case of the 4mpz derivative, the third crop of product afforded the desired material free of impurities.

Preparation of $[Rh_2(\mu\text{-dppm})_2Cl_2(CO)_2(\mu\text{-X})]PF_6$ (X = 4-Chloropyrazolate (4Cpz), 4-Chloro-3,5-dimethylpyrazolate (4C35mpz), 4mpz). The following is a typical synthesis of the chloro derivatives. Chlorine gas was bubbled through a stirred CH_2Cl_2 solution of 180 mg (0.145 mmol) of $[Rh_2(\mu\text{-dppm})_2(CO)_2(\mu\text{-pz})]PF_6$ at 0 °C in the absence of UV light. The volume of the yellow solution was reduced to ca. 10 mL, and 50 mL of ether was added to give a yellow solid, which was collected by filtration and recrystallized from CH_2Cl_2/ether and dried in vacuo.

The Cl_2 was prepared by introducing 5 mL of 12 M HCl (62.0 mmol) into a flask containing 1.22 g of $KMnO_4$ (7.75 mmol). The Cl_2 was bubbled through concentrated H_2SO_4 (200 mL) before reacting with the appropriate complex. Residual Cl_2 was neutralized by bubbling it into 6 M NaOH.

(1) The groups of the periodic table are numbered according to recent recommendations of the IUPAC and ACS committees on nomenclature. Under this numbering system, the previous group V becomes group 15.
(2) (a) Puddephatt, R. J. *Chem. Soc. Rev.* **1983**, *12*, 99. (b) Balch, A. L. In *Homogeneous Catalysis with Metal Phosphine Complexes*; Pignolet, L. G., Ed.; Plenum: New York, 1984; Chapter 5.
(3) Sanger, A. R. In *Homogeneous Catalysis with Metal Phosphine Complexes*; Pignolet, L. G., Ed.; Plenum: New York, 1984; Chapter 6.
(4) (a) Oro, L. A.; Pinillos, M. T.; Tiripicchio, A.; Tiripicchio-Camellini, M. *Inorg. Chim. Acta* **1985**, *99*, L13. (b) Uson, R.; Oro, L. A.; Ciriano, M. A.; Pinillos, M. T.; Tiripicchio, A.; Tiripicchio-Camellini, M. *J. Organomet. Chem.* **1981**, *205*, 247. (c) Powell, J.; Kuksis, A.; Nyburg, C.; Ng, W. W. *Inorg. Chim. Acta* **1982**, *64*, L211. (d) Uson, R.; Oro, L. A.; Ciriano, M. A.; Carmona, D.; Tiripicchio, A.; Tiripicchio-Camellini, M. *J. Organomet. Chem.* **1982**, *224*, 69.
(5) Oro, L. A.; Carmona, D.; Perez, P. L.; Esteban, M.; Tiripicchio, A.; Tiripicchio-Camellini, M. *J. Chem. Soc., Dalton Trans.* **1985**, 973.
(6) Enlow, P.; Woods, C. *Organometallics* **1983**, *2*, 64.
(7) Cowie, M.; Mague, J. T.; Sanger, A. R. *J. Am. Chem. Soc.* **1978**, *100*, 3628.

Physical Measurements. UV–vis spectra were recorded on a Cary 219 spectrophotometer. Infrared (IR) spectra were obtained with a Perkin-Elmer 1330 IR spectrophotometer. All IR spectra were obtained as Nujol mulls sealed between polyethylene sheets. All $^{31}P\{^1H\}$ NMR spectra were recorded on a JEOL FX90Q Fourier transform spectrometer at 36.19 MHz with 85% H_3PO_4 as the external reference. All electrochemical measurements were made relative to the saturated calomel electrode (SCE). Details of the equipment and techniques used for electrochemistry have been given elsewhere.[8]

Elemental analyses were performed by Galbraith Laboratories, Inc., Knoxville, TN. All complexes submitted for analyses gave satisfactory results.

X-ray Structure Determination of $[Rh_2(\mu\text{-dam})_2(CO)_2(\mu\text{-35mpz})]PF_6\cdot 0.75CH_2Cl_2$ (19). Ruby-colored prismatic crystals of **19** were grown by slow diffusion of ether into a CH_2Cl_2 solution of **19**. A representative crystal was cut to size (0.25 × 0.30 × 0.40 mm), and a 1-Å data set (maximum $(\sin\theta)/\lambda = 0.5$) was collected on a Syntex P1 diffractometer. The diffractometer was equipped with a graphite monochromator and molybdenum radiation (λ = 0.71069 Å). Final unit cell dimensions were obtained by a least-squares fit of 14 high-angle reflections ($2\theta > 18°$). Systematic absences indicated that the crystal belonged to the monoclinic space group $P2_1/c$ ($h0l$, $l = 2n + 1$; $0k0$, $k = 2n + 1$).[9] One check reflection collected every 30 reflections revealed no unexpected variation in intensity. A total of 6975 reflections were recorded in the following range of hkl: $-11 \le h \le 11$, $0 \le k \le 28$, $0 \le l \le 22$ ($5° < 2\theta < 42°$). The structure analysis was performed with use of 4451 of these reflections having $I > 3\sigma(I)$. Atomic scattering factors were taken from ref 10. All crystallographic calculations were performed with use of the Nicolet XTL and SHELXTL 5.1 structure solving package on a Nicolet R3m/μ crystallographic system.[11] All diffractometer data were collected at room temperature.

A trial structure containing rhodium, phosphorus, arsenic, fluorine, and some carbon atoms was obtained from direct methods. Subsequent difference Fourier maps revealed locations of the remaining atoms. This trial structure was refined routinely. Hydrogen positions were calculated. The hydrogen parameters were added to the structure factor calculations but were not refined. Methylene chloride found in the lattice was assigned a population of 77% after refining the site occupancy factors of Cl(1), Cl(2), and C(58) of the methylene chloride. Least-squares refinement showed that this model fit the data well. The final cycles of block-diagonal-matrix least squares contained the scale factor, coordinates, and anisotropic temperature factors. An extinction correction was applied and refined to a value of zero. A final difference Fourier map revealed no peaks larger than those that could be assigned to hydrogen atoms, with the largest $\Delta/\sigma = 0.12$. The data fit criteria (based on 4451 non-zero reflections and 695 non-zero parameters) were $R = \sum(|F_o| - |F_c|)/\sum|F_o| = 0.0665$, $R_w = [[\sum w(|F_o| - |F_c|)^2]/\sum w|F_o|^2]^{1/2} = 0.0653$, and GOF = $[\sum w(|F_o| - |F_c|)^2/(N_o - N_v)]^{1/2} = 1.99$.

Complete tables of interatomic bond distances, bond angles, anisotropic thermal parameters, fractional atomic coordinates, hydrogen atom coordinates, and structure factors are available as supplementary material.

Results and Discussion

The addition of *n*-BuLi to the pyrazole derivatives and triazole produces the corresponding pyrazolate and triazolate anions. When these anions are added to $[Rh_2(\mu\text{-EE}')_2(CO)_2(\mu\text{-Cl})]PF_6$, complexes **1–4** and **13–20** are obtained. All of the dicarbonyl complexes except one show two strong IR bands between 1960 and 1991 cm^{-1}.[12] When 1 equiv of *t*-BuNC is added to complexes **1–4**, a new series of complexes, **5–8**, that have been formulated as containing one carbon monoxide and one isocyanide is obtained. The CO stretching frequencies for these mixed-ligand complexes occur between 1960 and 1980 cm^{-1}, and the NC stretching frequencies occur between 2122 and 2133 cm^{-1}.[12] The addition of 2 equiv of *t*-BuNC to complexes **1–4** results in the replacement of both carbon monoxide ligands. The infrared spectra of the diisocyanide complexes, **9–12**, exhibit two NC stretching frequencies between 2110 and 2125 cm^{-1}.[12]

The $^{31}P\{^1H\}$ NMR spectra of the dicarbonyl and the diisocyanide dppm complexes exhibit the symmetrical second-order AA′A″A‴XX′ pattern that is characteristic of symmetrical complexes containing two trans-bridging dppm ligands.[13] The spacings between the two major peaks, $^1J(Rh\text{–}P) + {}^xJ(Rh\text{–}P)$, occur at approximately 128 ± 2 Hz for the dicarbonyl complexes and 131 ± 3 Hz for the diisocyanide complexes. The $^{31}P\{^1H\}$ NMR patterns of the mixed-carbonyl–isocyanide complexes are asymmetric multiplets.

All of the dapm complexes give $^{31}P\{^1H\}$ spectra that contain an intense doublet, and a weaker doublet at slightly lower field. It has been previously shown that when the asymmetric dapm ligand is used to form dirhodium complexes, the head-to-head (HH) and head-to-tail (HT) isomers can result with the HT isomer being the predominant one.[6,14] Therefore, the major peaks in the $^{31}P\{^1H\}$ NMR spectra of the dapm dicarbonyl complexes have been assigned to the HT isomers (structure I where E = P and E′ = As). The fact that both the HT and HH isomers give a simple doublet indicates that either long-range Rh–P coupling is negligible or that second-order effects are small.

As with some previously reported dppm dimers containing pyrazolate derivatives,[5] the triazolate derivatives react with I_2 to give the Rh(II)–Rh(II) diiodides of structure IV. The increase in CO stretching frequency expected upon increasing the oxidation state of the metal is observed.

The UV–vis data show some interesting trends when the carbonyl ligands of the complexes $[Rh_2(\mu\text{-dppm})_2(CO)_2(X)]PF_6$ (X = pz, 4mpz, 35mpz, trz) are substituted with isocyanide ligands (Table II) and when dapm and dam are substituted for dppm in the dicarbonyl pz, 4mpz, 35dmpz, and trz complexes (Table III). It has been suggested[5] that the lowest energy electronic transition observed for these complexes is a "proximity shifted" transition[15] often observed when two rhodium metals are brought face to face to form dinuclear complexes. The data in Table III show that the lowest energy electronic transition of the dicarbonyl dppm complexes containing the pz, 4mpz, and 35mpz ligands moves to lower energy as the carbonyl ligands are replaced sequentially with *t*-BuNC ligands. The addition of *t*-BuNC therefore causes a decrease in the separation of the HOMO and LUMO. The data in Table III indicate that as one goes from the dppm to the dapm to the dam analogous complexes, the lowest energy electronic transition moves to higher energy. Thus, the addition of an arsenic donor atom to the methylene-bridged bidentate ligand leads to an increase in the separation of the HOMO and LUMO. One likely contribution to this increased HOMO–LUMO separation

Table II. Lowest Energy UV–Vis Transitions for $[Rh_2(\mu\text{-dppm})_2(\mu\text{-X})(L)(L')]PF_6$ Complexes

	λ_{max}, nm		
X	L, L′ = CO	L = CO, L′ = *t*-BuNC	L, L′ = *t*-BuNC
pz	492	505	514
4mpz	493	506	514
35dmpz	484	496	505
trz	487	493	504

Table III. Lowest Energy UV–Vis Transitions for $[Rh_2(\mu\text{-EE}')_2(CO)_2(\mu\text{-X})]PF_6$ Complexes

X	EE′	λ_{max}, nm	X	EE′	λ_{max}, nm
pz	dppm	492	35dmpz	dpm	484
	dapm	483		dapm	478
	dam	476		dam	471
4mpz	dppm	493	trz	dppm	487
	dapm	483		dapm	478
	dam	476		dam	469

(8) Janke, C. J.; Tinsley, P. W.; Tortorelli, L. J.; Woods, C., submitted for publication in *Inorg. Chem.*
(9) *International Tables for Crystallography*; Hahn, T., Ed.; D. Reidel: Dordrecht, Holland, 1983; Vol. A.
(10) *International Tables for X-ray Crystallography*; Kynoch: Birmingham, England, 1962; Vol. IV, pp 55, 99, 149.
(11) *Nicolet SHELXTL Structure Determination Manual*; Sheldrick, G. M., Ed.; Nicolet Instrument Corp.: Madison, WI, 1983.
(12) Tables containing more extensive IR, NMR, and UV–vis data are available in Tables SI and SII as supplementary material.
(13) Mague, J. T.; Sanger, A. R. *Inorg. Chem.* **1979**, *18*, 2060.
(14) Guimerans, R. R.; Balch, A. L. *Inorg. Chim. Acta* **1983**, *77*, L177.
(15) Balch, A. L. *J. Am. Chem. Soc.* **1976**, *98*, 8049.

Table IV. $^{31}P\{^1H\}$ NMR Data for $[Rh_2(\mu\text{-dppm})_2(CO)_2(\mu\text{-X})(Z)_2]PF_6$ Complexes

X	Z	δ	X	Z	δ
pz	I	4.82	4mpz	Cl	11.35
	Br[a]	8.93	35 mpz	I	6.40
	Cl[a]	10.68		Br[a]	10.98
4mpz	I	4.89		Cl[a]	13.44
	Br	8.93			

[a] The pyrazolate derivative of the parent dimer was halogenated at position 4 of the ring.

is the decrease in orbital overlap resulting from the increase in bite size as one goes from dppm to dapm to dam. The reduced overlap of the d_{z^2} orbitals should contribute to a lowering of the HOMO, and the reduced overlap of the p_z orbitals should contribute to a raising of the LUMO.[16] Electronic factors could also play a role in establishing the observed trend; however, at this time it is not clear to what extent the variation of the HOMO–LUMO separation is due to changes in structural or electronic factors. This issue is currently being investigated.

Reaction of $[Rh_2(\mu\text{-dppm})_2(CO)_2(\mu\text{-X})]PF_6$ (X = pz, 4mpz, 35mpz) with Chlorine and Bromine. Addition of Br_2 to complexes **1–3** leads to orange or yellow solids exhibiting IR bands in the 2000-cm^{-1} region,[12] indicative of the presence of terminal CO ligands. These bromination products were expected to be the simple oxidative-addition products analogous to those obtained upon addition of iodine to complexes **1–3**. However, the analytical data are consistent with the addition of three bromine atoms in the case of **1** and **3** and the expected two bromine atoms in the case of **2**. The $^{31}P\{^1H\}$ NMR spectra of all three bromination products exhibit the symmetrical AA'A''A'''XX' pattern. The analytical and spectroscopic data led us to formulate the bromination products of **1**, **2**, and **3** as complexes **25**, **26**, and **27**, respectively. It is interesting to note that the 35mpz and pz ligands are brominated in position 4, which is blocked in 4mpz. To support our formulation of complexes **25** and **27**, we performed an electrochemical reductive-elimination reaction on **27**. Under these conditions it was expected that the bromine atoms coordinated to the Rh centers would be eliminated during the reduction from Rh(II) to Rh(I), whereas the bromine atom in position 4 of the ring would remain. The cyclic voltammogram of **27** shows an irreversible reduction wave at −0.34 V (vs. SCE). Controlled-potential electrolysis at −0.65 V is a two-electron process and produces an orange complex whose IR spectrum exhibits CO stretching frequencies in the terminal CO region that are about 60 cm^{-1} lower than those of the starting material. Such a decrease is expected in going from Rh(II) to Rh(I) due to an increase in back-bonding. The $^{31}P\{^1H\}$ NMR spectrum of the reduction product contains the expected AA'A''A'''XX' pattern. The analytical data, which confirm the presence of one bromine atom per dinuclear species, and the spectroscopic data are consistent with the formulation of the reduction product as **31**. The spectroscopic data of **31** are identical with those of an authentic sample prepared from the commercially available 4-bromo-3,5-dimethylpyrazole.

Chlorination gives results analogous to those of the bromination reactions; thus, complexes **1**, **2**, and **3** give complexes **28**, **29**, and **30**, respectively. Electrochemical reductive elimination of the chloro ligands from **30** is achieved by controlled-potential electrolysis at −0.65 V. Similarly, the product retains a chlorine atom and is formulated as **32**. The analytical data for the chlorination products **28**, **29**, and **30** and the reduction product **32** are best interpreted with a 0.25 mol of CH_2Cl_2 present per dinuclear unit. The analogous iodides and some other similar dirhodium species crystallize with four dinuclear units per unit cell; thus, a molecule of CH_2Cl_2 per unit cell would be consistent with the above interpretation of the analytical data.

The values of $^1J(Rh\text{–}P) + {}^xJ(Rh\text{–}P)$ for the Rh(I) dicarbonyl complexes **1–4** occur at 128 ± 2 Hz. These values decrease to 83 ± 2 Hz upon halogenation to form the Rh(II) dinuclear dicarbonyl complexes.[12] The ^{31}P chemical shifts for the halogenated pz, 4mpz, and 35mpz Rh(II) complexes display an interesting trend (Table IV). For a given pyrazolate derivative, the chemical shifts increase in the order I < Br < Cl. The variation in δ(P) with halogen substitution observed here is opposite to that observed for some other metal phosphine derivatives recently reported.[17] It has been noted[18] that chemical shift relationships do not reflect phosphorus electron density changes in a simple manner and that, over a large range of compounds, empirical correlations of such shifts break down.

Structure of $[Rh_2(\mu\text{-dam})_2(CO)_2(\mu\text{-35mpz})]PF_6\cdot 0.75CH_2Cl_2$ (19). Shortly after we initiated a structure analysis of **19**, the structure of the bis(phosphine)-bridged analogue **3** was reported.[2] Since the two complexes have different donor atoms, we felt it might still be of interest to complete the analysis of **19**. The structure of **19** and the numbering scheme are shown in Figure 1. Atomic coordinates and selected bond distances and angles are given in Tables V and VI, respectively. In view of the facts that the structural integrities of the two complexes are the same and that many structural parameters are similar, we report here only a limited number of the details of our analysis of **19**;[19] other details of the structure determination are available as supplementary material. There are, however, a few structural comparisons that are worth noting.

The larger size of the arsenic atom compared to that of the phosphorus atom imparts a larger bite size on dam than on dppm. This is expected to lead to a greater Rh···Rh separation in the diarsine-bridged dimers. This is verified by the Rh···Rh distance of 3.220 Å in **19** compared to 3.060 Å in **3**. As noted earlier, such a variation in Rh···Rh separation undoubtedly plays a role in establishing the differences observed in the electronic properties of the two series of complexes. It is interesting to note that though the Rh···Rh separation is larger in **19**, the N(1)–N(2) bond distances in **19** and **3** are the same within experimental error. The Rh–N distances are also similar, 2.08 (1) and 2.07 Å for **3** and 2.103 (13) and 2.088 (10) Å for **19**. The increase in the Rh···Rh separation of **19** is consistent with an increase in the dihedral angle between the least-squares plane containing Rh(1), N(1), and C(1) and the least-squares plane containing Rh(2), N(2), and C(2). The Rh–N–N angles in the two complexes are 118.3 (8) and 114.2 (8)° for **19** and 115 (1) and 113 (1)° for **3**. The adjacent Rh–N–C angles are necessarily smaller for **19**, 133.0 (11) and 135.8 (9)°, than for **3**, 138 (1) and 139 (1)°, respectively. A simple approximate calculation gives the angles between the extended Rh(1)–N(1) and Rh(2)–N(2) vectors. As one goes from **3** to **19**, the values of these angles, approximately 48° for **3** and 53° for **19**, also reflect the opening of the dihedral angle between the least-squares planes containing these vectors.

Conclusions

Several new dirhodium A-frame complexes containing triazolate and pyrazolate derivatives in the bridgehead position have been synthesized and characterized. Sequential substitution of isocyanide ligands for terminal carbon monoxide ligands in these complexes leads to systematic variations in the HOMO–LUMO separation. This variation is almost certainly due to electronic factors that depend on the different bonding capabilities of the carbon monoxide and isocyanide ligands. The HOMO–LUMO separation is also dependent on the nature of the methylene-bridged bidentate ligand. The substitution of a larger arsenic atom for a phosphorus atom has been shown to lead to a larger bite size for the bridging ligand and therefore a larger Rh···Rh separation. This variation in Rh···Rh separation with size of the donor

(16) Fordyce, W. A.; Crosby, G. A. *J. Am. Chem. Soc.* **1982**, *104*, 985.

(17) Hohman, W. H.; Kountz, D. J.; Meek, D. W. *Inorg. Chem.* **1986**, *25*, 616.

(18) Verkade, J. G. *Coord. Chem. Rev.* **1972/1973**, *9*, 1.

(19) Crystal data for **19**: $C_{57}H_{51}As_4F_6N_2O_2PRh_2\cdot{}^3/_4CH_2Cl_2$, space group $P2_1/c$, a = 10.259 (2) Å, b = 27.577 (7) Å, c = 21.485 (7) Å, β = 103.15 (2)°, V = 5919 (2) Å^3, μ(Mo Kα) = 29.42 cm^{-1}, Z = 4, F(000) = 3023, D_{measd} = 1.58 g cm^{-3}, D_{calcd} = 1.60 g cm^{-3}.

Table V. Atomic Coordinates ($\times 10^4$) and Isotropic Thermal Parameters ($\times 10^3$ Å^2)[a]

atom	x	y	z	U	atom	x	y	z	U
Rh(1)	2341 (1)	1907 (1)	3016 (1)	37 (1)*	C(21)	−174 (18)	844 (7)	3323 (8)	63 (8)*
Rh(2)	1710 (1)	1720 (1)	1496 (1)	35 (1)*	C(22)	464 (15)	3016 (6)	2369 (7)	44 (6)*
As(1)	2559 (2)	1061 (1)	3280 (1)	37 (1)*	C(23)	377 (15)	3500 (6)	2190 (7)	53 (7)*
As(2)	2198 (2)	2716 (1)	2700 (1)	36 (1)*	C(24)	−944 (26)	3701 (8)	1939 (11)	103 (12)*
As(3)	2265 (1)	2547 (1)	1240 (1)	35 (1)*	C(25)	−2039 (21)	3408 (9)	1930 (9)	118 (12)*
As(4)	1696 (2)	865 (1)	1758 (1)	37 (1)*	C(26)	−1920 (23)	2941 (9)	2119 (13)	127 (14)*
P	4707 (5)	4341 (2)	2028 (3)	58 (2)*	C(27)	−656 (16)	2713 (8)	2336 (8)	68 (8)*
Cl(1)	8325 (12)	3032 (4)	3949 (6)	179 (7)*	C(28)	2912 (16)	3214 (5)	3372 (7)	44 (6)*
Cl(2)	8774 (9)	4037 (3)	4170 (5)	136 (5)*	C(29)	4185 (18)	3374 (7)	3456 (8)	65 (8)*
F(1)	4467 (11)	4881 (4)	2230 (5)	92 (5)*	C(30)	4690 (22)	3671 (8)	3980 (11)	93 (11)*
F(2)	5518 (14)	4215 (5)	2710 (7)	142 (7)*	C(31)	3929 (25)	3837 (8)	4389 (10)	80 (10)*
F(3)	4906 (10)	3807 (4)	1780 (6)	97 (6)*	C(32)	2655 (26)	3661 (7)	4296 (10)	82 (10)*
F(4)	3883 (12)	4465 (5)	1321 (6)	107 (6)*	C(33)	2132 (18)	3348 (7)	3782 (8)	64 (8)*
F(5)	3316 (10)	4167 (4)	2169 (6)	95 (5)*	C(34)	1047 (15)	3040 (5)	781 (7)	41 (6)*
F(6)	6007 (11)	4524 (4)	1830 (7)	104 (6)*	C(35)	−271 (15)	2952 (6)	537 (8)	53 (7)*
C(1)	1101 (18)	1993 (7)	3484 (8)	71 (8)*	C(36)	−1082 (16)	3305 (7)	204 (9)	72 (8)*
O(1)	298 (14)	2051 (5)	3777 (6)	97 (7)*	C(37)	−562 (20)	3727 (7)	65 (9)	78 (9)*
C(2)	−46 (18)	1745 (6)	1136 (8)	60 (7)*	C(38)	754 (19)	3814 (6)	270 (8)	62 (8)*
O(2)	−1178 (13)	1767 (5)	863 (10)	150 (9)*	C(39)	1614 (17)	3476 (5)	660 (8)	57 (7)*
N(1)	3977 (10)	1800 (4)	2597 (6)	35 (5)*	C(40)	3623 (13)	2581 (5)	744 (6)	34 (6)*
N(2)	3729 (11)	1688 (4)	1963 (6)	33 (5)*	C(41)	3279 (17)	2502 (6)	98 (8)	55 (7)*
C(3)	3109 (14)	2879 (5)	2007 (6)	40 (6)*	C(42)	4234 (19)	2488 (7)	−261 (8)	70 (9)*
C(4)	2938 (13)	700 (5)	2576 (7)	40 (6)*	C(43)	5569 (19)	2538 (7)	39 (9)	65 (9)*
C(5)	5311 (15)	1776 (6)	2839 (8)	50 (7)*	C(44)	5932 (16)	2615 (7)	670 (8)	72 (9)*
C(6)	5884 (14)	1622 (6)	2326 (7)	50 (7)*	C(45)	4970 (15)	2639 (7)	1039 (8)	59 (7)*
C(7)	4850 (14)	1578 (5)	1801 (6)	37 (6)*	C(46)	109 (14)	488 (5)	1783 (7)	41 (6)*
C(8)	4940 (15)	1413 (6)	1148 (7)	51 (7)*	C(47)	232 (18)	−0 (6)	1915 (10)	81 (10)*
C(9)	5973 (15)	1891 (6)	3505 (7)	54 (7)*	C(48)	−919 (21)	−285 (7)	1890 (10)	83 (10)*
C(10)	4025 (15)	922 (5)	4013 (7)	42 (6)*	C(49)	−2137 (19)	−66 (9)	1805 (8)	76 (10)*
C(11)	4035 (16)	1168 (6)	4574 (7)	50 (7)*	C(50)	−2217 (19)	417 (8)	1706 (10)	83 (10)*
C(12)	5020 (20)	1083 (7)	5117 (9)	71 (9)*	C(51)	−1170 (16)	711 (7)	1680 (8)	64 (8)*
C(13)	5949 (19)	740 (7)	5107 (8)	65 (8)*	C(52)	2338 (15)	464 (5)	1115 (7)	37 (6)*
C(14)	5978 (17)	482 (7)	4548 (10)	77 (9)*	C(53)	3558 (17)	214 (6)	1291 (9)	62 (8)*
C(15)	5017 (15)	577 (6)	4003 (8)	59 (7)*	C(54)	3941 (19)	−39 (7)	798 (9)	66 (8)*
C(16)	1126 (15)	686 (5)	3505 (7)	36 (6)*	C(55)	3200 (22)	−60 (7)	200 (11)	74 (10)*
C(17)	1378 (19)	261 (7)	3832 (9)	74 (9)*	C(56)	1978 (19)	188 (7)	42 (8)	65 (8)*
C(18)	382 (18)	−14 (7)	3969 (10)	84 (9)*	C(57)	1578 (17)	458 (6)	496 (9)	57 (8)*
C(19)	−906 (24)	108 (9)	3760 (9)	84 (11)*	C(58)	8315 (29)	3631 (10)	3708 (15)	118 (16)*
C(20)	−1167 (18)	536 (7)	3435 (9)	84 (9)*					

[a] Values marked with an asterisk are equivalent isotropic U values defined as one-third of the trace of the orthogonalized U_{ij} tensor.

Table VI. Selected Bond Distances (Å) and Angles (deg)

(a) Bonded Distances

Rh(1)–As(1)	2.400 (2)	Rh(1)–As(2)	2.406 (2)
Rh(1)–C(1)	1.809 (20)	Rh(1)–N(1)	2.098 (12)
Rh(2)–As(3)	2.444 (2)	Rh(2)–As(4)	2.425 (2)
Rh(2)–C(2)	1.794 (17)	Rh(2)–N(2)	2.088 (10)
As(1)–C(4)	1.923 (15)	As(2)–C(3)	1.963 (15)
As(3)–C(3)	1.911 (13)	As(4)–C(4)	1.974 (12)
C(1)–O(1)	1.155 (26)	C(2)–O(2)	1.177 (21)
N(1)–N(2)	1.311 (19)		

(b) Nonbonded Distances

Rh(1)–Rh(2)	3.220	As(2)–As(3)	3.199
As(1)–As(4)	3.234		

(c) Angles

As(1)–Rh(1)–As(2)	176.5 (1)	As(1)–Rh(1)–C(1)	92.0 (6)
As(2)–Rh(1)–C(1)	91.5 (6)	As(1)–Rh(1)–N(1)	85.7 (3)
As(2)–Rh(1)–N(1)	91.0 (3)	C(1)–Rh(1)–N(1)	171.9 (6)
As(3)–Rh(2)–As(4)	166.8 (1)	As(3)–Rh(2)–C(2)	97.5 (5)
As(4)–Rh(2)–C(2)	94.5 (5)	As(3)–Rh(2)–N(2)	83.8 (3)
As(4)–Rh(2)–N(2)	84.5 (3)	C(2)–Rh(2)–N(2)	177.0 (7)
Rh(1)–As(2)–C(3)	112.6 (4)	Rh(2)–As(3)–C(3)	109.6 (4)
Rh(2)–As(4)–C(4)	113.1 (4)	Rh(1)–C(1)–O(1)	179.1 (14)
Rh(2)–C(2)–O(2)	175.7 (19)	Rh(1)–N(1)–N(2)	118.3 (8)
Rh(2)–N(2)–N(1)	114.1 (8)	As(2)–C(3)–As(3)	111.3 (7)
As(1)–C(4)–As(4)	112.1 (7)	Rh(1)–N(1)–C(5)	133.0 (11)
Rh(2)–N(2)–C(7)	135.8 (9)		

atom of the methylene-bridged bidentate ligand should affect the extent of orbital overlap of the two metal d_{z^2} and p_z orbitals and, hence, the HOMO–LUMO separation. This could explain a structural dependence of the lowest energy electronic transition; however, a simultaneous electronic dependence cannot be ruled out since phosphorus and arsenic do have slightly different donor properties.

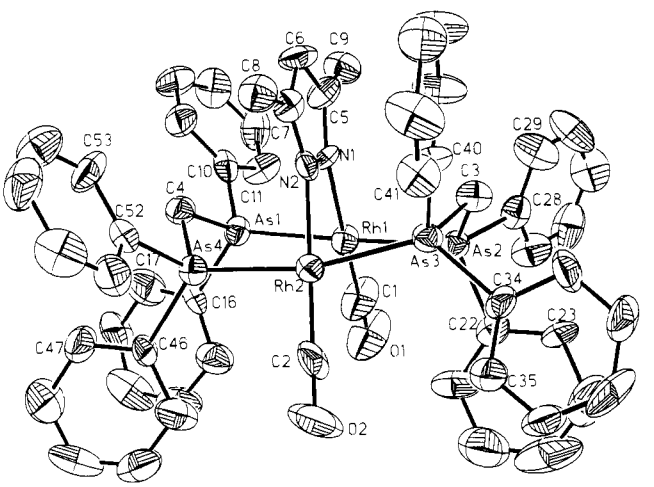

Figure 1. ORTEP plot of $[Rh_2(\mu\text{-dam})_2(CO)_2(\mu\text{-35mpz})]^+$. The hydrogen atoms have been omitted for clarity, and the carbon atoms in the phenyl rings are numbered sequentially around the ring.

Acknowledgment. We wish to thank the National Science Foundation for support of this work and Johnson Matthey, Inc., for a generous loan of rhodium trichloride. We also appreciate the helpful comments of Dr. Phirtu Singh of North Carolina State University.

Supplementary Material Available: IR and NMR data for compounds **1–32** (Table SI), UV-vis data for compounds **1–32** (Table SII), bond

lengths (Table SIII), bond angles (Table SIV), anisotropic thermal parameters (Table SV), and H atom coordinates and isotropic thermal parameters (Table SVI) (10 pages); observed and calculated structure factors (Table SVII) (38 pages). Ordering information is given on any current masthead page.

Contribution from the Department of Chemistry, University of Exeter, Exeter EX4 4QD, England

Extended Hückel Calculations and the Role of d Orbitals in Transition-Metal-Cluster Bonding

D. G. Evans

Received February 12, 1986

In two recent articles in this journal, Woolley[1,2] has suggested that the metal d electrons play a crucial role in the bonding between transition-metal atoms in clusters and furthermore[2] that the extended Hückel (EH) model offers no explanation for the metal–metal bonding in such clusters. While the first statement would receive general support from chemists, the second is clearly more contentious. In the light of the important advances in our understanding of cluster chemistry furnished by Hoffmann,[3] Mingos,[4] and others[5] that have been supported by calculations of this type, it is desirable to examine the validity of Woolley's argument[2] in some detail. Some early EH calculations[5,6] suggested that the d bands in clusters were rather narrow, and this was interpreted in terms of the d electrons making a very minor contribution to the metal–metal bonding. It is the purpose of this note to demonstrate that a detailed examination of the results from a number of EH calculations can satisfactorily account for the bonding in such clusters and *indeed* does highlight the important contribution made by the metal d electrons. The relationship between the conclusions derived here and the qualitative predictions of Woolley[1,2] based on the methodology of metal physics will also be discussed. Finally it will be clearly demonstrated within the framework of perturbation theory how the symmetry of the ligand field induces an interplay between the metal s, p, and d electrons that is not present in the bare metal cluster. This enables an ambiguity, left unresolved in the metal physics predictions,[1,2] to be understood.

EH calculations[7] on the neutral bare metal clusters Fe_5 and Ru_5 (both trigonal bipyramidal)[8] and octahedral[8] Co_6 have been performed with the usual metal parameters[3,9] and Wolfsberg–Helmholtz constant (K = 1.75).[7] It must be emphasised that contrary to the claims of Woolley,[1,2] the parameters have not been deliberately "chosen" to give artificially high metal d–d overlap integrals. Thus for example in the case of Fe_5 all such values are 0.051 or less, consistent with the ideas of metal physics. The calculations show that the atomic d orbitals overlap to give a band of $5n$ levels (for an M_n cluster) of width 1.7–3.0 eV. These are also of the order considered reasonable by Woolley (at least 2.2 eV)[1] for metal d bands in bare metal clusters. (The introduction of a ligand shell leads to an increase in d-band width as discussed below.) In each case the overlap of the valence s and p orbitals is larger as a consequence of their greater spatial extension giving a much wider spread of levels. One of these, derived from metal s orbitals (which we shall call S_s^σ in the notation of tensor surface harmonic theory,[10] TSH), lies embedded in the d band, and the other $4n - 1$ levels lie well above the d band. Clearly the exact nature of the metal–metal bonding will depend on whether S_s^σ lies above or below the Fermi level of the cluster. With any reasonable EH parameterization, S_s^σ and the Fermi level are very close in energy, and in Table I we summarize the percentage contribution of each type of orbital overlap to the computed Mulliken overlap population for the three clusters, assuming first that S_s^σ lies above and second that it lies below the Fermi level. In each case the s–s, s–p and p–p orbital overlaps make a relatively minor (0–36%) contribution to the metal–metal bonding (in Woolley's view[1,2] the valence s and p orbitals actually give rise to a small antibonding contribution), and the major component of the metal–metal bonding arises from interactions involving the metal d orbitals. This is contrary to the impression given elsewhere[5,6] that EH calculations ascribe the metal–metal bonding to overlap between s and p orbitals. Further indication of the minor role ascribed to the s and p orbitals by the EH method comes from the calculated atomic orbital populations. If the S_s^σ level is assumed to be unoccupied, these are, for example

$$Fe_5 \quad s^{0.29}\, d^{7.63}\, p^{0.09}$$

$$Ru_5 \quad s^{0.12}\, d^{7.82}\, p^{0.06}$$

and even if the S_s^σ level is assumed to be occupied there is relatively little change. For example, the calculations give

$$Fe_5 \quad s^{0.52}\, d^{7.39}\, p^{0.09}$$

Consider now the introduction of a set of ligands to such a cluster. The electron count of the resulting species may be predicted by using the criterion of Lauher;[5] viz., there will be a large energy gap between the cluster HOMO and LUMO in the region close to the p orbital energy in an isolated atom. This gives total electron counts of 72 and 86, respectively, for the trigonal bipyramid and the octahedron as is well-known.[4] In a 72-electron cluster such as $Fe_5X_5^{22-}$, (where X represents a two-electron ligand with the orbital exponent and H_{ii} of hydrogen),[9] the cluster d band orbitals do not interact significantly with the ligands, and complete occupation of the d band gives a net antibonding contribution to the metal–metal interaction. In this case, and in this highly

Table I. Percentage of Total Overlap Population Arising from Overlap between Individual Sets of Metal Atomic Orbitals for a Series of Pentanuclear Clusters[a]

	percentage of total overlap population arising from each type of orbital overlap					
cluster	s–s	s–p	p–p	s–d	p–d	d–d
Fe_5 (S^σ vacant)	11	2	0	30	22	35
Fe_5 (S^σ occupied)	29	2	0	21	19	29
Ru_5 (S^σ vacant)	−1	−2	−1	34	24	45
Ru_5 (S^σ occupied)	30	0	0	19	13	39
Co_6 (S^σ vacant)	0	1	−1	40	42	19
Co_6 (S^σ occupied)	36	3	0	21	22	18
Fe_5^{32-}	1	30	73	5	0	−9
$Fe_5X_5^{22-}$	11	37	54	5	3	−9
$Fe_5X_{15}^{2-}$	10	22	21	10	29	9
$Fe_5(CO)_{15}^{2-}$	3	11	18	13	40	16

[a] A negative value indicates an antibonding contribution to the metal–metal-overlap population.

(1) Woolley, R. G. *Inorg. Chem.* **1985**, *24*, 3519.
(2) Woolley, R. G. *Inorg. Chem.* **1985**, *24*, 3525.
(3) Hoffmann, R. *Angew. Chem., Int. Ed. Engl.* **1982**, *21*, 711 and references therein.
(4) Mingos, D. M. P. *Acc. Chem. Res.* **1984**, *17*, 311.
(5) Lauher, J. W. *J. Am. Chem. Soc.* **1978**, *100*, 5305.
(6) Mingos, D. M. P. *J. Chem. Soc. A* **1974**, 133.
(7) Hoffmann, R. *J. Chem. Phys.* **1963**, *39*, 1397.
(8) Bond lengths (Å) used in the calculations: Fe–Fe = 2.53; Ru–Ru = 2.854; Co–Co = 2.50; Fe–X = 1.60.
(9) EH parameters: Fe 4s ζ = 1.90, H_{ii} = −9.17 eV; 4p ζ = 1.90, H_{ii} = −5.37 eV; 3d ζ_1 = 5.35 (c_1 = 0.5366), ζ_2 = 1.80 (c_2 = 0.6678), H_{ii} = −12.70 eV; Ru 5s ζ = 2.078, H_{ii} = −8.00 eV; 5p ζ = 2.043, H_{ii} = −4.3 eV; 4d ζ_1 = 4.21 (c_1 = 0.5772), ζ_2 = 1.95 (c_2 = 0.5692), H_{ii} = −12.20 eV; Co 4s ζ = 2.00, H_{ii} = −9.21 eV; 4p ζ = 2.00 H_{ii} = −5.29 eV; 3d ζ_1 = 5.55 (c_1 = 0.5679), ζ_2 = 2.10 (c_2 = 0.6059), H_{ii} = −13.18 eV; X 1s ζ = 1.30, H_{ii} = −13.60 eV.
(10) Stone, A. J. *Inorg. Chem.* **1981**, *20*, 563.

0020-1669/86/1325-4602$01.50/0